Joint estimation of CFOs and Doppler shifts in mmWave distributed MIMO systems

David Demmer, Valentin Savin, Nicola Di Pietro, Jean-Baptiste Doré

Joint estimation of CFOs and Doppler shifts in mmWave distributed MIMO systems

David Demmer*, Valentin Savin*, Nicola di Pietro†, Jean-Baptiste Doré*

*CEA-LETI, Université Grenoble Alpes, F-38000 Grenoble, France
{david.demmer, valentin.savin, jean-baptiste.dore}@cea.fr

† Athonet Srl, via Cà del Luogo 6/8, 36050, Bolzano Vicentino (VI), Italy
nicola.dipietro@athonet.com

***Abstract*—Distributed Multiple Input Multiple Output (MIMO) systems, where the base stations (BSs) have several Radio Units (RUs) that are spatially distributed around the cell, are considered in this study. With such an architecture, each wireless link between the RUs and the devices experiences a different frequency offset. This accumulation of frequency offsets degrades the reconstruction of the coherent downlink signals at the receiver side and therefore limits the system capacity. Such frequency offsets are unavoidable, due to both independent local oscillators inducing Carrier Frequency Offsets (CFOs) and moving devices inducing Doppler shifts. The problem becomes more critical in millimeter wave (mmWave) communications because of large Doppler shifts even for low device speed. Estimating the frequency offsets at the device side requires the simultaneous estimations of multiple frequency offsets which can be computationally intensive. In this study we propose to move the estimation problem at the BS side so that the frequency offsets can be compensated for the downlink which eases the recombination of the precoded signals at the device side. To properly compensate the frequency offsets at each wireless link, the different sources of frequency offset must be jointly estimated. A joint CFOs and Doppler shifts estimation is first described and asymptotically analysed. The paper also includes a performance evaluation of the proposed joint estimation technique. It appears that significant performance gains are achieved for realistic systems. It makes the proposed solution interesting for some beyond 5G MIMO scenarios like indoor reliable industry connectivity or vehicular communications.**

***Index Terms*—spatially distributed MIMO systems, Doppler effect, frequency offset estimation and compensation**

I. Introduction

Wireless connectivity is making its way into industrial networks as it is *plug and play*, eases the maintenance and control of devices, and even enables the coordination of moving devices such as transport vehicles. Sub-GHz bands are not suitable to support a dense traffic and their reliability can be significantly reduced because of the presence of interfering systems. That is why millimeter wave (mmWave) spectrum is considered as a plausible candidate to replace wires in industrial sectors especially with the licensed band at 28 GHz and the unlicensed band at 60 GHz [1]. However, wireless communications are unreliable compared to wired links and poor connectivity can result in delayed transmission or reduced performance. The challenge is thus to ensure Ultra Reliable and Low Latency Communications (URLLC) wirelessly which is critical for industrial applications.

In industrial environments, Radio Frequency (RF) blockages may occur in mmWave communications because of moving objects and vehicles. Spatial diversity is therefore required to prevent those RF blockages [2]. In this context, distributed MIMO systems, also known as Cell-Free MIMO, have been proposed to improve the system capacity of conventional co-localized systems [3]. With such architectures, the Base Station (BS) is composed of a Centralized Unit (CU) responsible for the digital signal processing and several Radio Units (RUs) that are spatially distributed over the cell and responsible for the RF processing of the signals. In this work, we consider beamforming techniques at the RUs side to come up with severe path loss of the millimeter wireless links. The main advantages of the distributed architecture are i) providing an improved coverage thanks to an enhanced channel diversity and higher robustness to RF blockages and ii) less path loss and energy consumption thanks to shorter BS-device distances in average [4], [5]. The uplink signals are received by one or more RUs which transpose it into the baseband and forward it to the CU for reconstruction. This is known as joint reception. When it comes the downlink, the CU precodes the signal to transmit to the devices and send the resulting signals to the RUs for over-the-air transmission. The devices thus receive a set of coherent signals to recombine for reconstruction. It is known as joint transmission. The way to precode the downlink messages depends on the system. It can be for instance linear schemes like Zero-Forcing or Minimum Mean Square Error to mitigate the inter-user interference in Multi-User MIMO (MU-MIMO).

This work addresses the challenges related to the downlink of distributed MU-MIMO systems. In those systems, the downlink signals experience different frequency offsets. First, those frequency offsets are partially induced by the independent local oscillators of the RUs and the devices. This effect is known as Carrier Frequency Offset (CFO). Then when the devices move, the Doppler effect also adds a frequency offset which even differs for each wireless link. Those frequency offsets are critical impairments in mmWave

This work has been supported by CPS4EU project, which has received funding from the ECSEL Joint Undertaking (JU) under grant agreement N°826276.
Nicola di Pietro was with CEA-Leti when this study was conducted.

communications as large shifts occur because of the high carrier frequencies. To reconstruct the downlink signal, the devices must perform the estimation of multiple frequency offsets in order to compensate them. Some techniques based on training sequences exist and some of them can even approach Maximum Likelihood (ML) performance [6]. However, those iterative algorithms are rather computationally intensive and are therefore not suitable for devices with limited computation resources or links with stringent latency constraints like there can be in the case of industrial networks.

In this study, we move the estimation at the BS side based on measurements of the uplink signals like in [7]. It is worth noticing that because of the sparsity of the propagation channel, the Doppler effect is reduced to simple Doppler shifts like the CFOs. The overall frequency offset experienced on each link is thus the sum of the contribution of the CFOs and the Doppler shifts. However, the overall frequency offsets, including CFOs and Doppler shifts, are not the same on the uplink and the downlink, as it will be discussed in the section dedicated to the description of the system model. It is therefore required to jointly estimate the CFOs and the Doppler shifts for each wireless links in order to properly compensate those effects for the downlink.

The remainder of this paper is organized as follows. The system model is described and the important notions defined in Section II. In Section III, we introduced a regression model for the joint estimation of the frequency offsets. A theoretical analysis is also provided. Then, the performance of the proposed estimator and the resulting performance at the system-level are evaluated in Section IV. Finally, perspective studies and concluding remarks are given in Section V.

II. System Model

The BS is composed of N RUs responsible for the transmission/reception of wireless signals and one CU performing the signal processing. Each RU is equipped with an antenna array and is able to perform a beamforming with beam width α. The K devices are equipped with omnidirectional antenna. In this study, we assume that the antenna array is able to steer its beam in the direction of the maximum received power, either in Line-of-Sight (LOS) or non-LOS. The multi-path components of the propagation channel are then filtered out by the RU beamforming [8]. The received signal is thus only composed of one resolvable path along with L_p unresolvable paths. Besides, the RUs are static which implies that the Doppler effect is due to the mobility of the devices. However, the AoDs are equal for all the unresolvable paths between device i and RU j, and therefore the Doppler shift is the same. As a consequence, a simpler propagation channel model with a unique unresolvable path will be assumed for the rest of the paper. Nonetheless, the Doppler shift experienced on each device-RU link varies because the AoDs are different.

In addition to the Doppler effect, the frequency shift induced by oscillator imperfections are taken into consideration as well. f_j^{RU} and f_i^{UE} respectively denote the CFOs of the RU j and the device i. The system model for two RUs and two devices is depicted in Figure 1. For the RU, a common

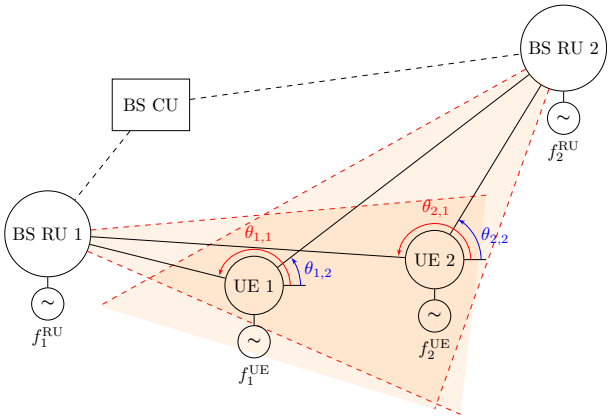

Figure 1. System model with two UEs.

clock signal can be obtained with a network synchronization protocol like Global Navigation Satellite Systems (GNSS) or Time Sensitive Networking (TSN) which is becoming more and more central in industrial Internet of Things (IoT). And when the synchronization provided by the protocol is not sufficient, other over-the-air synchronization procedures can be considered [9]. Therefore, the clock imperfection of the RUs will be neglected for this study: $f_j^{RU} = 0$ for any RU j.

The resulting frequency offset experienced on the uplink path between device i and the RU j is thus the sum of the contributions of the device CFO f_i^{UE} and the Doppler shift $f_{i,j}^{DOP}$:

$$\Delta f_{i,j}^{UL} = f_i^{UE} + f_{i,j}^{DOP} \tag{1}$$

The Doppler shift expression is given in (2) where v_i denotes the device speed, f_s the carrier frequency of the signal, c the light celerity, $\theta_{i,j}$ the AoD of the link and ϕ_i the device angular direction.

$$f_{i,j}^{DOP} = \frac{v_i f_s}{c} \cos\left(\theta_{i,j} - \phi_i\right) \tag{2}$$

When it comes to the frequency offset experienced on the downlink for the same path, one obtains the expression (3). The overall frequency offset experienced on the link depends on the same terms but with the opposite contribution for the device CFO. Indeed, as the relative motion of the device with respect to each RU is the same for both links then the Doppler shift is also the same on both UL and DL links. To obtain this expression, it is assumed that the time interval between the uplink and downlink signals is small enough so that the CFO and the device localisation remain constant which is a reasonable assumption.

$$\Delta f_{i,j}^{DL} = -f_i^{UE} + f_{i,j}^{DOP} \tag{3}$$

This observation justifies the need of a joint CFO and Doppler shift estimation on each wireless link. It is indeed required to estimate separately the contributions of f_i^{UE} and $f_{i,j}^{DOP}$ to properly estimate the overall frequency offset. We propose in this study, a joint estimation technique based on measurements from the uplink signals. The resulting estimation of the downlink frequency offset $\Delta f_{i,j}^{DL}$ can thus be

used to compensate the phase variation of the Channel State Information (CSI) induced by time delay between the CSI and the DL precoding.

One can observe that the estimation problem can be performed independently for each device. The estimation problem introduced in (1) can thus be simplified to a single-device problem where the index i is omitted:

$$\Delta f_j = f^{UE} + f^{DOPm} \cos\left(\theta_j - \phi\right). \tag{4}$$

III. Joint-estimation algorithm

A. Regression problem

We aim at estimating the device CFO f^{UE}, the maximum Doppler shift f^{DOPm} and the angular direction of the device ϕ based on the measurements of the AoD of the wireless uplink signals θ_j at each RU and the cumulated frequency shifts Δf_j.

On the one hand, the quality of the measurement for the frequency shifts depends on many parameters: the signal-to-noise ratio of the wireless link, the reference signals (preamble structure [10], pilot-based [11], blind [12] and so on). Given that our objective is to assess the feasibility and the performance in ideal conditions, the overall frequency shift measurement is assumed to be ideal.

On the other hand, the measurement of the AoDs cannot be ideal. Indeed, the AoD is measured at each RU thanks to the angle-domain projection of the signal [7] obtained with the antenna arrays. The measurements of the AoDs, denoted $\widehat{\theta}_j$, are then noisy and the accuracy depends of the beam width α:

$$\widehat{\theta}_j = \theta_j + \epsilon_j \tag{5}$$

where ϵ_j denotes a random noise that we assume follow a uniform continuous distribution $\mathcal{U}(-\alpha/2, \alpha/2)$.

The regression problem described in (4) is non-linear and therefore not easy to solve. We propose here a pragmatic solution to linearize the problem by using trigonometric relations:

$$\begin{aligned}\Delta f_j = f^{UE} &+ f^{DOPm} \cos\left(\phi\right) \cos\left(\widehat{\theta}_j\right) \\ &+ f^{DOPm} \sin\left(\phi\right) \sin\left(\widehat{\theta}_j\right).\end{aligned} \tag{6}$$

The expression (6) can be put in the matrix form as well:

$$\mathbf{\Delta f} = \mathbf{X}\widehat{\mathbf{Y}} \tag{7}$$

where

- $\mathbf{\Delta f} = [\Delta f_1, \ldots, \Delta f_N] \in \mathbb{R}^{1\times N}$
- $\mathbf{X} = [f^{UE}; f^{DOPm}\cos(\phi); f^{DOPm}\sin(\phi)] \in \mathbb{R}^{1\times 3}$
- $\widehat{\mathbf{Y}} \in \mathbb{R}^{3\times N}$ with j^{th} column $\widehat{Y}_j = [1; \cos(\widehat{\theta}_j); \sin(\widehat{\theta}_j)]^T$

Lemma 1: Assume that $N \geq 3$, and AoDs $\theta_1, \ldots, \theta_N$ are independent and uniformly distributed in $[0, 2\pi]$. Then, $\widehat{\mathbf{Y}}$ is full rank with probability 1.

The proof of Lemma 1 is given in Appendix A.

As a consequence, when $N \geq 3$ $\widehat{\mathbf{Y}}\widehat{\mathbf{Y}}^{\mathbf{T}}$ is invertible with probability 1 and $\widehat{\mathbf{X}}$ can be evaluated by applying (8).

$$\widehat{\mathbf{X}} = \mathbf{\Delta f}\widehat{\mathbf{Y}}^T \left(\widehat{\mathbf{Y}}\widehat{\mathbf{Y}}^T\right)^{-1}. \tag{8}$$

Finally, the estimation of the three parameters of interests can be expressed as follows:

$$\widehat{f}^{UE} = \widehat{X}(1) \tag{9}$$

$$\widehat{f}^{DOPm} = \sqrt{\widehat{X}(2)^2 + \widehat{X}(3)^2} \tag{10}$$

$$\widehat{\phi} = \operatorname{atan}\left(\frac{\widehat{X}(3)}{\widehat{X}(2)}\right) \tag{11}$$

where $X(i)$ is the i-th coordinate of the vector $\mathbf{X}$.

B. Analytical analysis

The theoretical performance of the estimator is discussed in this section.

By inserting (7) into (8), one obtains:

$$\widehat{\mathbf{X}} = \mathbf{X}\mathbf{Y}\widehat{\mathbf{Y}}^{\mathbf{T}} \left(\widehat{\mathbf{Y}}\widehat{\mathbf{Y}}^{\mathbf{T}}\right)^{-1} \tag{12}$$

$$= \mathbf{X}\left(\frac{1}{N}\mathbf{Y}\widehat{\mathbf{Y}}^T\right)\left(\frac{1}{N}\widehat{\mathbf{Y}}\widehat{\mathbf{Y}}^T\right)^{-1} \tag{13}$$

The following lemma is proved in Appendix B.

Lemma 2: Assume that AoDs $\theta_1, \ldots, \theta_N$ are independent and uniformly distributed in $[0, 2\pi]$. Then, the following equalities hold with probability 1.

1) $\lim\limits_{N\to\infty} \frac{1}{N}\widehat{\mathbf{Y}}\widehat{\mathbf{Y}}^{\mathbf{T}} = \begin{pmatrix} 1 & 0 & 0 \\ 0 & 1/2 & 0 \\ 0 & 0 & 1/2 \end{pmatrix}$

2) $\lim\limits_{N\to\infty} \frac{1}{N}\mathbf{Y}\widehat{\mathbf{Y}}^{\mathbf{T}} = \frac{1}{N}\begin{pmatrix} 1 & 0 & 0 \\ 0 & \frac{1}{\alpha}\sin(\frac{\alpha}{2}) & 0 \\ 0 & 0 & \frac{1}{\alpha}\sin(\frac{\alpha}{2}) \end{pmatrix}$

By using the above lemma, one gets:

$$\lim_{N\to\infty} \widehat{\mathbf{X}} = \mathbf{X}\begin{pmatrix} 1 & 0 & 0 \\ 0 & \frac{2}{\alpha}\sin(\frac{\alpha}{2}) & 0 \\ 0 & 0 & \frac{2}{\alpha}\sin(\frac{\alpha}{2}) \end{pmatrix}. \tag{14}$$

It implies that

$$\lim_{N\to\infty} \widehat{f}^{UE} = f^{UE} \tag{15}$$

$$\lim_{N\to\infty} \widehat{f}^{DOPm} = \frac{2}{\alpha}\sin(\frac{\alpha}{2}) f^{DOPm} \tag{16}$$

$$\lim_{N\to\infty} \widehat{\phi} = \phi \tag{17}$$

It means that the estimators (9) and (11) are consistent but (10) is not. However, by setting (18), one gets (19).

$$\widehat{\widehat{f}}^{DOPm} = \frac{\alpha}{2\sin\left(\frac{\alpha}{2}\right)} \widehat{f}^{DOPm} \tag{18}$$

$$\lim_{N\to\infty} \widehat{\widehat{f}}^{DOPm} = f^{DOPm} \tag{19}$$

We have then defined three consistent estimators for the parameters of interest (9), (18) and (11). It means that by considering the system model presented in (4) when one collects a large number of measurements of frequency offsets, the three estimators converge in probability to the true value of the parameters independently of the value of the RU beam width α.

C. Summary of the proposed algorithm

1) At time t_0, a CSI estimation for the downlink wireless links $H_i(t_0)$ is performed at the BS side. This part is not detailed in this paper and several techniques can be used such as in-band pilot symbols for Time-Division Duplexing (TDD) systems by assuming channel reciprocity or out-of-band pilot symbols for Frequency Division Duplexing (FDD) systems.
2) At time $t \geq t_0$, the device sends an uplink signal which is received by the spatially distributed RUs. Each RU performs the RF processing and downconverts it into the baseband. The baseband signal is then sent to the BS CU.
3) At time t, the CU determines for each received uplink signal the angle of arrival (based on the active beam) $\widehat{\mathbf{Y}}$ and measures the overall frequency offset $\mathbf{\Delta f}$.
4) At time t, from the collection of measurements obtained in 3), the CU performs the estimation of the device CFO $\widehat{f}^{UE}$, the device max Doppler shift $\widehat{f}^{DOPm}$ and the device angular direction $\widehat{\phi}$ by applying (8) and respectively (9), (18) and (11).
5) At time $t_1 \geq t \geq t_0$, the CU predicts the channel variation based on the estimation performed in 4) as expressed in (20) and then can precode the downlink signals by using the resulting CSI. The precoding technique is not detailed in this paper and several techniques can be used such as the Zero-Forcing to avoid inter-user interference.

$$H_i(t_1) = H_i(t_0) e^{2i\pi\left(-\widehat{f}^{UE} + \widehat{f}^{DOPm}\cos(\widehat{\theta}_i - \widehat{\phi})(t_1 - t_0)\right)} \quad (20)$$

IV. Performance Evaluation

In this section, the algorithm performance is evaluated for practical scenarios (*i.e.* with limited number of RUs). Three criteria will be assessed: i) the estimation accuracy of the parameters of interest, ii) the quality of the resulting channel prediction and iii) the achievable sum-rate.

An industry 4.0 scenario is considered for the simulations with an indoor scenario and wireless connectivity working at the 26.7 GHz licensed band [1]. The list of the simulation parameters is given in Table I. For the evaluation performance, the normalized Mean Square Error (nMSE) indicator is used in this study. Its expression is reminded in (21) where X and $\widehat{X}$ are respectively the real and the estimated scalar values of the parameter of interest, $|x|$ depicts the absolute value of the real x and $\mathbb{E}$ is the expectation operator.

$$\text{nMSE}(\widehat{X}) = \mathbb{E}\left(\frac{|\widehat{X} - X|^2}{|X|^2}\right) \quad (21)$$

The first performance indicator is the quality of the estimation technique for the three parameters of interest: the device CFO f^{UE}, the device max Doppler f^{DOPm} and the device angular direction ϕ (point 4) of III-C). The results are depicted in Figure 2. In the latter figure, the curves 'ϕ with $N = 16$' (blue diamonds) and 'f^{DOPm} with $N = 16$' (green diamonds) are superimposed.

Table I
Simulation parameters

Indoor scenario	
Room dimension	8×4 m
RUs	uniformly placed at the room borders
Signal	
Center frequency	26.7 GHz
CFO	0.1 ppm [13]
UEs	
Location	Uniformly distributed in the room
Speed	Uniformly distributed between 0 and 30 km/h
Direction	Uniformly distributed between 0 and 2π

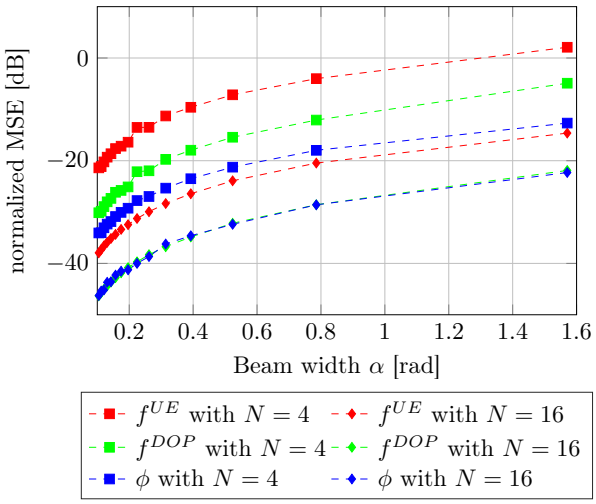

Figure 2. Evaluation of the estimation accuracy for two possible RU deployments $N = 4$ and $N = 16$.

One can observe the relative impact of the two parameters on the quality of the estimation: the number of RUs N (*i.e.* the number of measurements) and the beam width α (*i.e.* the accuracy of the measurement of the AoD). Recall that the cumulated frequency shifts Δf_j in (4) are ideally estimated. First, the estimators appears to be also consistent when α tends to 0 for any $N \geq 3$ which is another interesting asymptotic property of the proposed estimation technique. Moreover, for realistic values of α and N, α looks to play a more predominant role on the estimator accuracy. This implies that the quality of the estimation is better improved by narrowing the beam widths than by adding new RUs.

It seems interesting to notice that for a given configuration (fixed N and α), the accuracy of the estimation differs from one parameter to another. Indeed, the estimation of the CFO exhibits the largest error and the estimation of the device direction ϕ appears to be the most accurate of all. Indeed, an averaging effect occurs during the estimation of the device max Doppler shift f^{DOPm} (10) and the device direction ϕ (11) which improves the accuracy of the estimation.

Now, we can estimate the resulting accuracy of the channel prediction based on (20). The results are depicted in Figure 3 for 4, 8 and 16 RUs. Expectedly, the curves have similar

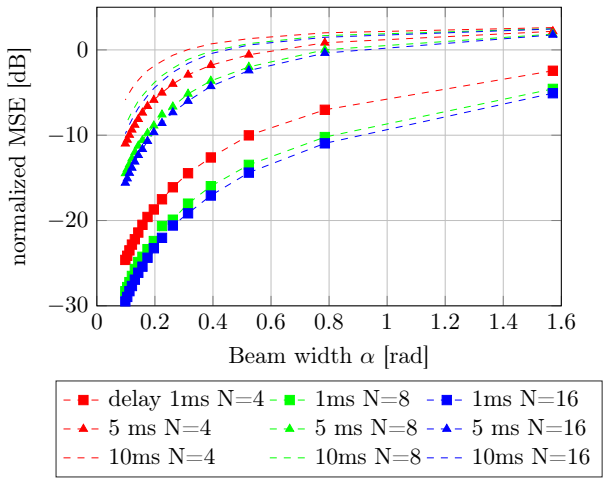

Figure 3. Evaluation of the error in the channel prediction.

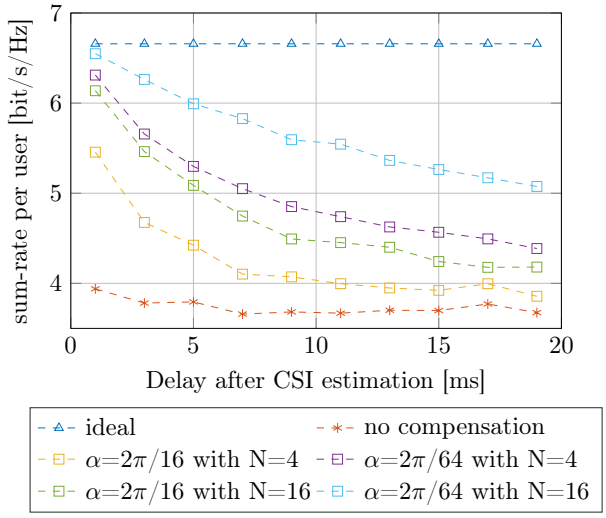

Figure 4. Achievable sum-rate.

variations that the ones of Figure 2. One can observe as well that the performance obtained with the proposed solution degrades with time. Indeed as the estimation is not perfect, the error on the estimation can accumulate with time. It implies that the estimates have a given validity in time and that for long delay of channel prediction the estimates can be outdated. Depending on the scenario and the traffic, the number of RUs and beam widths must be carefully selected to ensure a good channel prediction.

We can now evaluate the performance of the proposed solution at the system level with the results represented in Figure 4. The figure depicts the mean sum-rate that can be obtained with the configuration given in Table I. The expression of the mean sum-rate $\mathcal{R}$ is given in (22) where P_{sig}, P_{noi} and P_{int} respectively denote the powers of the received useful signal, the noise and the interference terms. The noise power if fixed to ensure a Signal-to-Noise Ratio (SNR) of 20 per link, *i.e.* $\frac{P_{\text{sig}}}{P_{\text{noi}}} = 20$ dB. The interference term comes from the inter-user interference from the zero-forcing precoding induced by the error of CSI due to imperfect channel prediction. The curves corresponding to the 'ideal' case, meaning perfect estimation and channel prediction and 'no compensation' case, meaning no estimation and channel prediction is performed, are plotted as well for comparison.

$$\mathcal{R}(t_1 - t_0) = \mathbb{E}\left(\log\left(1 + \frac{P_{\text{sig}}}{P_{\text{int}}(t_1 - t_0) + P_{\text{noi}}}\right)\right) \quad (22)$$

As expected, the proposed solution improves the achievable sum-rate. The performance gains are significant for small delays and even tend to the ideal sum rate. However, as observed with Figure 3, the quality of the estimation is limited in time and that is why the performance gap with respect to the ideal case increases with the delay. The gain in performance is still substantial for a delay of 10 ms, typical frame duration in 5G systems, with 127% increase for $\alpha = 2\pi/64$ and $N = 4$ or 150% increase for $\alpha = 2\pi/64$ and $N = 16$.

V. Perspectives and Conclusion

We proposed a joint estimation technique to cope with the frequency offsets in a multi-user distributed MIMO systems. The estimation is performed at the BS side to keep the device processing as simple as possible. The proposed solution takes into consideration device mobility, thus it is inherently robust to Doppler effect. No condition on the channel delay spread or a-priori knowledge of device directions is required, which is a real advantage with respect to similar solutions proposed in the literature. The proposed estimation technique has suitable asymptotic properties and provides significant performance gains with both realistic and practical scenarios. It makes the proposed solutions appealing for beyond 5G MU-MIMO scenarios.

In this paper, strong assumptions have been made (ideal frequency estimates and perfect RU oscillator synchronization). Those assumptions lead to a simple system model which is interesting for a first approach but their impacts on the achievable performance will be analysed and evaluated in a future publication.

References

[1] D. Solomitckii, A. Orsino, S. Andreev, Y. Koucheryavy, and M. Valkama, "Characterization of mmWave Channel Properties at 28 and 60 GHz in Factory Automation Deployments," in *Proc. IEEE Wireless Communications and Networking Conference (WCNC)*, April 2018.

[2] M. Khoshnevisan, V. Joseph, P. Gupta, F. Meshkati, R. Prakash, and P. Tinnakornsrisuphap, "5G Industrial Networks With CoMP for URLLC and Time Sensitive Network Architecture," *IEEE Journal on Selected Areas in Communications*, vol. 37, no. 4, pp. 947–959, April 2019.

[3] N. H. Dawod, I. D. Marsland, and R. H. M. Hafez, "Improved transmit null steering for MIMO-OFDM downlinks with distributed base station antenna arrays," *IEEE Journal on Selected Areas in Communications*, vol. 24, no. 3, pp. 419–426, 2006.

[4] H. Q. Ngo, A. Ashikhmin, H. Yang, E. G. Larsson, and T. L. Marzetta, "Cell-Free Massive MIMO Versus Small Cells," *IEEE Transactions on Wireless Communications*, vol. 16, no. 3, pp. 1834–1850, 2017.

[5] Y. Zhao, I. G. Niemegeers, and S. H. De Groot, "Distributed mmWave Massive MIMO: A Performance Comparison with a Centralized Architecture for Various Degrees of Hybridization," in *IEEE International Conference on Information, Communication and Networks (ICICN)*, 2020, pp. 105–110.

[6] B. W. Zarikoff and J. K. Cavers, "Multiple Frequency Offset Estimation for the Downlink of Coordinated MIMO Systems," *IEEE Journal on Selected Areas in Communications*, vol. 26, no. 6, pp. 901–912, 2008.
[7] R. Zeng, H. Huang, L. Yang, and Z. Zhang, "Joint Estimation of Frequency Offset and Doppler Shift in High Mobility Environments Based on Orthogonal Angle Domain Subspace Projection," *IEEE Transactions on Vehicular Technology*, vol. 67, no. 3, pp. 2254–2266, March 2018.
[8] T. S. Rappaport, G. R. MacCartney, M. K. Samimi, and S. Sun, "Wideband Millimeter-Wave Propagation Measurements and Channel Models for Future Wireless Communication System Design," *IEEE Transactions on Communications*, vol. 63, no. 9, pp. 3029–3056, 2015.
[9] R. Rogalin, O. Y. Bursalioglu, H. Papadopoulos, G. Caire, A. F. Molisch, A. Michaloliakos, V. Balan, and K. Psounis, "Scalable Synchronization and Reciprocity Calibration for Distributed Multiuser MIMO," *IEEE Transactions on Wireless Communications*, vol. 13, no. 4, pp. 1815–1831, April 2014.
[10] Jian Li, Guoqing Liu, and G. B. Giannakis, "Carrier frequency offset estimation for OFDM-based WLANs," *IEEE Signal Processing Letters*, vol. 8, no. 3, pp. 80–82, 2001.
[11] M. Speth, S. A. Fechtel, G. Fock, and H. Meyr, "Optimum receiver design for wireless broad-band systems using OFDM. I," *IEEE Transactions on Communications*, vol. 47, no. 11, pp. 1668–1677, 1999.
[12] G. D. Pantos, "A numerical technique for blind estimation of carrier frequency offset in ofdm systems," *IEEE Transactions on Broadcasting*, vol. 52, no. 4, pp. 566–569, 2006.
[13] 3GPP, "Technical Specification Group Radio Access Network; User Equipment (UE) radio transmission and reception; Part 2: Range 2 Standalone (Release 16)," 3rd Generation Partnership Project (3GPP), techreport TR 38.101-2, Mar. 2020, version 16.3.0.

APPENDIX A
PROOF OF LEMMA 1

It is enough to prove the statement for $N = 3$, since $\Pr(\mathrm{rank}(\widehat{\mathbf{Y}}) = 3)$ is a non-decreasing function of N. For $N = 3$, we have

$$\det(\widehat{\mathbf{Y}}) = \sin(\widehat{\theta}_2 - \widehat{\theta}_1) + \sin(\widehat{\theta}_3 - \widehat{\theta}_2) + \sin(\widehat{\theta}_1 - \widehat{\theta}_3) \quad (23)$$

$$= 4 \sin\left(\frac{\widehat{\theta}_1 - \widehat{\theta}_2}{2}\right) \sin\left(\frac{\widehat{\theta}_2 - \widehat{\theta}_3}{2}\right) \sin\left(\frac{\widehat{\theta}_3 - \widehat{\theta}_1}{2}\right) \quad (24)$$

where the first equality is obtained by direct computation, and the second follows easily from well known sum-to-product trigonometric identities. Therefore $\det(\widehat{\mathbf{Y}}) = 0$ if and only if $\widehat{\theta}_i = \widehat{\theta}_j$ or $\widehat{\theta}_i = \widehat{\theta}_j + \pi \mod 2\pi$, $\forall 1 \leq i \neq j \leq 3$, which happens with probability zero. Equivalently, $\det(\widehat{\mathbf{Y}}) \neq 0$, thus $\mathrm{rank}(\widehat{\mathbf{Y}}) = 3$, with probability 1, as desired.

APPENDIX B
PROOF OF LEMMA 2

First, we note that for a random variable θ, such that $\theta \mod 2\pi$ is uniformly distributed on $[0, 2\pi]$, we have

$$\mathbb{E}[\cos(\theta)] = \mathbb{E}[\sin(\theta)] = 0, \quad (25)$$

where $\mathbb{E}$ denotes the expectation operator, and therefore

$$\mathbb{E}\left[\cos^2(\theta)\right] = \mathbb{E}\left[\frac{1}{2}(1 + \cos(2\theta))\right] = \frac{1}{2} \quad (26)$$

$$\mathbb{E}\left[\cos^2(\theta)\right] = \mathbb{E}\left[\frac{1}{2}(1 - \cos(2\theta))\right] = \frac{1}{2} \quad (27)$$

$$\mathbb{E}\left[\sin(\theta)\cos(\theta)\right] = \mathbb{E}\left[\frac{1}{2}\sin(2\theta)\right] = 0 \quad (28)$$

Proof of 1) To prove the first limit, we note that

$$\widehat{\mathbf{Y}}\widehat{\mathbf{Y}}^{\mathbf{T}} = \begin{pmatrix} N & \sum_j \cos(\widehat{\theta}_j) & \sum_j \sin(\widehat{\theta}_j) \\ \sum_j \cos(\widehat{\theta}_j) & \sum_j \cos^2(\widehat{\theta}_j) & \sum_j \cos(\widehat{\theta}_j)\sin(\widehat{\theta}_j) \\ \sum_j \sin(\widehat{\theta}_j) & \sum_j \cos(\widehat{\theta}_j)\sin(\widehat{\theta}_j) & \sum_j \sin^2(\widehat{\theta}_j) \end{pmatrix}$$

Since $\widehat{\theta}_1, \widehat{\theta}_2 \ldots$ is an infinite sequence of independent random variables, with modulo 2π reduction uniformly distributed on $[0, 2\pi]$, it follows from (25)–(28) and the strong law of large numbers (LLN) that the first limit Lemma 2 holds with probability 1.

Proof of 2) To prove the second limit, we start with

$$\mathbf{Y}\widehat{\mathbf{Y}}^{\mathbf{T}} = \begin{pmatrix} N & \sum_j \cos(\widehat{\theta}_j) & \sum_j \sin(\widehat{\theta}_j) \\ \sum_j \cos(\theta_j) & \sum_j \cos(\theta_j)\cos(\widehat{\theta}_j) & \sum_j \cos(\theta_j)\sin(\widehat{\theta}_j) \\ \sum_j \sin(\theta_j) & \sum_j \cos(\widehat{\theta}_j)\sin(\theta_j) & \sum_j \sin(\theta_j)\sin(\widehat{\theta}_j) \end{pmatrix}$$

By the LLN, we have that $\frac{1}{N}\sum_j \cos(\theta_j)$, $\frac{1}{N}\sum_j \cos(\widehat{\theta}_j)$, $\frac{1}{N}\sum_j \sin(\theta_j)$, and $\frac{1}{N}\sum_j \sin(\widehat{\theta}_j)$ go to zero, as N goes to infinity. For the elements in positions (3,2) and (2,3) in $\mathbf{Y}\widehat{\mathbf{Y}}^{\mathbf{T}}$, we first note that

$$\sin(\widehat{\theta}_j)\cos(\theta_j) = \frac{1}{2}\left[\sin(\widehat{\theta}_j + \theta_j) + \sin(\widehat{\theta}_j - \theta_j)\right]$$

$$= \frac{1}{2}\left[\sin(2\theta_j + \epsilon_j) + \sin(\epsilon_j)\right] \quad (29)$$

$$\cos(\widehat{\theta}_j)\sin(\theta_j) = \frac{1}{2}\left[\sin(\widehat{\theta}_j + \theta_j) - \sin(\widehat{\theta}_j - \theta_j)\right]$$

$$= \frac{1}{2}\left[\sin(2\theta_j + \epsilon_j) - \sin(\epsilon_j)\right] \quad (30)$$

Since ϵ_j is uniformly distributed on $[-\alpha/2, \alpha/2]$, and $(2\theta_j + \epsilon_j \mod 2\pi)$ is uniformly distributed on $[0, 2\pi]$, we have $\mathbb{E}[\sin(\epsilon_j)] = \mathbb{E}[\sin(2\theta_j + \epsilon_j)] = 0$. Thus, invoking again the LLN, we obtain $\lim_{N\to\infty} \frac{1}{N}\sum_j \sin(\widehat{\theta}_j)\cos(\theta_j) = \lim_{N\to\infty} \frac{1}{N}\sum_j \cos(\widehat{\theta}_j)\sin(\theta_j) = 0$, with probability 1.

Finally, we proceed in a similar way for the diagonal elements in positions (2,2) and (3,3) in $\mathbf{Y}\widehat{\mathbf{Y}}^{\mathbf{T}}$, by first observing that:

$$\cos(\widehat{\theta}_j)\cos(\theta_j) = \frac{1}{2}\left[\cos(\epsilon_j) + \cos(2\theta_j + \epsilon_j)\right] \quad (31)$$

$$\sin(\widehat{\theta}_j)\sin(\theta_j) = \frac{1}{2}\left[\cos(\epsilon_j) - \cos(2\theta_j + \epsilon_j)\right] \quad (32)$$

Using $\mathbb{E}[\cos(\epsilon_j)] = \frac{2}{\alpha}\sin(\frac{\alpha}{2})$ and $\mathbb{E}[\cos(2\theta_j + \epsilon_j)] = 0$, we get with probability 1, $\lim_{N\to\infty} \frac{1}{N}\sum_j \cos(\widehat{\theta}_j)\cos(\theta_j) = \lim_{N\to\infty} \frac{1}{N}\sum_j \sin(\widehat{\theta}_j)\sin(\theta_j) = \frac{1}{\alpha}\sin\left(\frac{\alpha}{2}\right)$, which completes the proof.